Nested PPM for Visible Light Communication With Heterogeneous Optical Receivers

Jan Mietzner, *Senior Member, IEEE*, and Lutz Lampe, *Senior Member, IEEE*

***Abstract*—We consider visible light communication (VLC) using phosphorescent white light-emitting diodes (LEDs) and two different receiver types – a simple receiver for moderate data rate requirements and a sophisticated receiver for higher data rate requirements equipped with an optical blue filter. We address the question, whether it is viable to support both heterogeneous receiver types simultaneously, using a single LED-based transmitter, and characterize the trade-offs associated with a common waveform. In particular, with regard to a simplistic transmitter and receiver structure, we propose a "nested" pulse-position modulation (nPPM) scheme and show that it improves upon conventional time sharing, when the bit rate of the simple receiver is supposed to be retained, while realizing a higher bit rate for the sophisticated receiver. An analysis of the available signal-to-noise ratio at the receiver for a practical setting combined with analytical and simulated error performance results corroborates the feasibility of our approach. Furthermore, we devise an end-to-end signal model, which includes the electrical properties of the LED as well as interference effects associated with optical filtering, and assess the influence on the resulting error performance. Due to its simplicity, our nPPM scheme may be particularly relevant for future mass-market VLC deployments as well as for proprietary solutions.**

***Index Terms*—Visible light communication (VLC), optical filtering, pulse-position modulation (PPM), signal modeling, performance analysis.**

I. Introduction

VISIBLE light communication (VLC) – also referred to as LiFi, if bi-directional and fully networked – has been identified in recent years as a viable alternative or complement to wireless radio-frequency (RF) solutions, e.g., in environments with stringent electro-compatibility requirements or in settings with challenging data traffic demands [1], [2]. A particular advantage of VLC is its sustainability aspect, as existing infrastructure installed for lighting functions may be reused for wireless data transfer [3]. For a wide acceptance, however, additional hardware and software costs for the VLC function should be kept to a minimum [4].

Manuscript received 29 February 2024; revised 7 May 2024; accepted 23 May 2024. Date of publication 28 May 2024; date of current version 11 June 2024. *(Corresponding author: Jan Mietzner.)*

Jan Mietzner is with the Faculty of Design, Media and Information, Hamburg University of Applied Sciences (HAW), 20099 Hamburg, Germany, and also with the Department of Electrical & Information Engineering (ECE), The University of British Columbia (UBC), Vancouver, BC V6T 1Z4, Canada (e-mail: jan.mietzner@haw-hamburg.de).

Lutz Lampe is with the Department of Electrical & Information Engineering (ECE), The University of British Columbia (UBC), Vancouver, BC V6T 1Z4, Canada (e-mail: lampe@ece.ubc.ca).

Digital Object Identifier 10.1109/JPHOT.2024.3406156

VLC relies on light-emitting diodes (LEDs), where the driving direct current (DC) is superimposed with a small-scale data signal. In earlier standardization efforts, on-off-keying (OOK) and pulse-position-modulation (PPM) waveforms with variable duty cycle were proposed, among others [5]. These were later extended by optical orthogonal-division multiplexing (OOFDM) waveforms [6], [7], mainly due to their potential of supporting higher bit rates. While OOFDM is employed in some commercially available LiFi products, a deep market penetration has not yet been attained. This is partly due to the fact that optical receiver modules have not yet been integrated into mass-market products, such as laptops, tablets, or smart phones. Another reason is that advanced modulation schemes, such as OOFDM, require digital signal synthesis at the transmitter side and fast-Fourier-transform based digital signal processing at the receiver side, which necessitates additional (and specialized) hardware components compared to a basic illumination system. Furthermore, OOFDM schemes typically require non-linear pre-distortion techniques at the transmitter side, in order to be compatible with the limited dynamic range of (standard) LEDs [1, Ch. 3].

With these limitations in mind, this paper aims to revisit more basic modulation schemes for VLC. In particular, we focus on PPM for the following reasons:

- PPM admits an extremely simplistic transmitter structure, which in essence comprises a software-controlled fast switch for generating transmitted pulses and a standard LED driver circuit.
- Signal dynamics are easily controlled, as PPM signals possess a well-defined maximum amplitude level.
- PPM also enables simple receiver processing, as long as pulse lengths are chosen such that intersymbol interference (ISI) effects are largely avoided. In particular, a conventional integrate-&-dump (I&D) receiver may be employed.
- PPM signals are inherently suitable for flicker-free VLC operation, whereas alternative modulation schemes (such as OOK) require additional line coding [5].

Especially with regard to future mass market products, as well as proprietary VLC solutions, PPM-based modulation schemes thus seem attractive, as they entail low additional infrastructure cost.

A downside of PPM is its limited bit rate, however, as pulse lengths circumventing ISI effects are restricted by the electrical bandwidth of the LED. In particular, state-of-art lighting systems usually employ phosphorescent white-light LEDs, due to their excellent color rendering properties [4]. Such luminaires employ

a green- or blue-light core LED with a phosphor coating – typically an yttrium aluminium garnett (YAG).[1] Regarding VLC, the phosphor is characterized by a relatively slow response time, resulting in a limited electrical bandwidth within the range of a few megahertz, whereas the core LED has considerably faster switching capabilities [2, Ch. 8.1]. VLC receivers typically employ photodiodes with an integrated optical filter for ambient light and infrared suppression [2, Ch. 8.2.1]. Additionally, narrowband optical filters may be employed, which are tailored to the spectrum emitted by the LED (see, e.g., [1, Ch. 2.4.2] and the references therein). In order to increase the bit rates for phosphorescent white-light LEDs, the electrical bandwidth can be increased by employing a dedicated optical blue filter at the receiver side [8], which suppresses the slow phosphor component of the optical spectrum – albeit at the expense of reducing the received optical power [9]. Typically, narrowband optical filters are relatively costly. In practice, there may thus be two user groups – one group with moderate data rate requirements, using a simple receiver without dedicated optical filter, and one requiring higher data rates, using a more sophisticated receiver with optical blue filter. Within the scope of this paper, we address the following question: Is it viable to support both heterogeneous receiver types simultaneously, using a single LED-based transmitter and a common waveform? Furthermore, under the premise that the already limited bit rate of the simple receiver should not be compromised, which trade-off can be attained, in order to offer a preferably high bit rate for the sophisticated receiver? To this end, we propose a hierarchical modulation scheme based on PPM – dubbed "nested" PPM (nPPM). We show, that the nPPM scheme is able to retain the bit rate of the simple receiver, while at the same time offering a bit rate for the sophisticated receiver which scales with the extended electrical bandwidth provided by the optical blue filter. Hierarchical modulation schemes are well established in wireless RF communication systems, e.g., for broadcasting applications [10] or relay-assisted networks [11]. For VLC, few hierarchical modulation schemes have been proposed, e.g., based on OOFDM [12], digital single-carrier modulation [13], [14], and coded color-shift keying [15] with the goal to improve the resilience and the performance of VLC systems. Our proposed nPPM scheme, however, addresses specific aspects associated with the use of white-light LEDs, while aiming for simple transmitter and receiver processing.

A. Contributions and Outline

The main contributions of the paper are as follows:

- Starting from an illumination perspective, we derive design guidelines for a hierarchical modulation scheme based on PPM. We show that our proposed nPPM scheme improves upon conventional time sharing, when the bit rate of the simple receiver is supposed to be retained (Section II).
- We provide analytical results regarding the attained error performance of nPPM for an ideal case without any interference, which serve as upper performance bounds (i.e., lower bounds on error rates). The resulting error performance is illustrated for selected examples, and the analytical results are validated by means of corresponding computer simulations (Section III).
- We devise an end-to-end system model, which accounts for heterogeneous optical receivers and interference effects due to non-perfect optical filtering. Based on this comprehensive model, we present numerical results illustrating the expected error performance of the nPPM scheme in practical scenarios with heterogeneous optical receivers (Section IV).

Possible extensions of nPPM are discussed in Section V. Conclusions are drawn in Section VI, and possible directions for future work are pointed out.

B. Mathematical Notation

Throughout, continuous-time signals are marked by round brackets (.) with time variable t, whereas discrete-time quantities, such as bit sequences, are marked by square brackets [.] with time index n. $\mathrm{rect}(t)$ denotes an ideal rectangular pulse with unit width and unit amplitude, which is centered around $t = 0$. The linear convolution of $x(t)$ and $y(t)$ is denoted as $x(t) * y(t) := \int_{-\infty}^{\infty} x(\tau) \cdot y(t-\tau)\,\mathrm{d}\tau$.

$\Pr\{\mathcal{E}\}$ denotes the probability of an event $\mathcal{E}$ and $x(t) \sim \mathcal{N}(0, \sigma^2)$ denotes a real-valued, zero-mean Gaussian distributed random process with variance σ^2. The Gaussian Q-function is given by $\mathrm{Q}(x) := 1/\sqrt{2\pi} \int_x^{\infty} \mathrm{e}^{-u^2/2}\,\mathrm{d}u$.

$\Theta(t)$ denotes the Heaviside function ($\Theta(t) = 0$ for all $t < 0$, $\Theta(0) = 0.5$, and $\Theta(t) = 1$ for all $t > 0$). Throughout, $\tilde{x}$ denotes a hypothesis for an information symbol x and $\hat{x}$ a corresponding hard decision. $\lfloor . \rfloor$ denotes rounding down to the next smaller integer value. Finally, $j = \sqrt{-1}$ denotes the imaginary unit.

II. System Model and Design Considerations

Lighting is the primary function of any VLC system and imposes corresponding side constraints on optical modulation schemes. In particular, for pulse-based modulation schemes the received symbol energy is directly determined by the desired illumination level. This can be seen when considering the VLC system model in Fig. 1. For the time being, we disregard the frequency responses of the LED and the photo detector (PD), i.e., $H_{\mathsf{LED}}(f) = H_{\mathsf{PD}}(f) = 1$. Moreover, we assume a non-dispersive VLC channel, i.e., $C(f) = 1$. In intensity-modulated/direct-detection (IM/DD) VLC systems, the transmitted information bits $d[n]$ are converted into a modulation signal $s(t)$, which is embedded in a time-varying LED driver current $i_{\mathsf{f}}(t)$ with mean $I_{\mathsf{DC,f}} > 0$. In Fig. 1, I_{ref} denotes a reference current and a_{tx} a suitable scaling factor. To avoid non-linear signal distortions, the driver current should be scaled such that its amplitude values are found within the dynamic range $[I_{\mathsf{min}}, I_{\mathsf{max}}]$ of the LED. Throughout this paper, we assume $I_{\mathsf{min}} = 0$ for the ease of exposition. Given a "monochromatic" LED (e.g., red, green, blue), the emitted optical power is then

[1]Throughout, we focus on a blue core LED with YAG coating, but our considerations are also relevant for other LEDs and phosphor types.

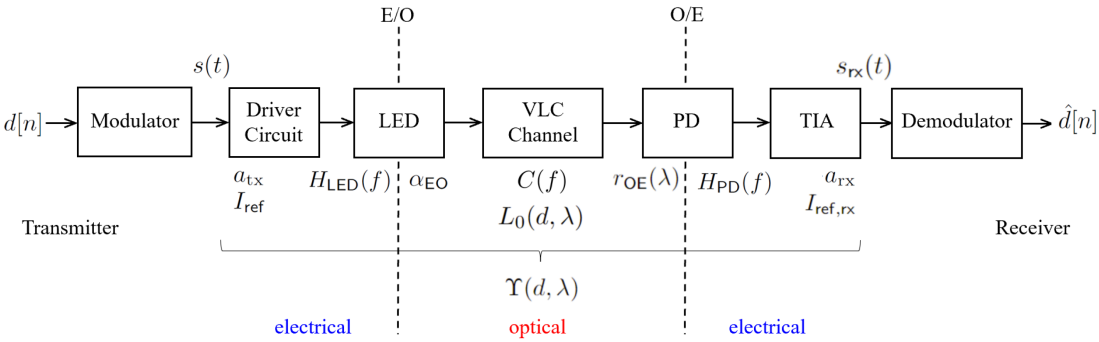

Fig. 1. VLC system model comprising the electrical domain and the signal domain.

proportional to the driver current, where α_{EO} denotes the corresponding proportionality factor in W/A associated with the electrical/optical (E/O) conversion [2, Ch. 3.6].

For a direct link between the LED and the PD, the received optical power is proportional to the transmitted optical power, where $L_0(d,\lambda) = (\lambda/(4\pi d))^2$ denotes the free-space propagation loss factor in the optical domain for a given optical wavelength λ and a distance d between the LED and the PD [2, Ch. 3.2]. The received optical power is captured by the PD, which generates a proportional photo current, where $r_{\mathsf{OE}}(\lambda)$ denotes the wavelength-dependent proportionality factor in A/W associated with the optical/electrical (O/E) conversion. Following the PD, a transimpedance amplifier (TIA) finally converts the photo current into a voltage signal [2, Ch. 9.2]. Throughout, we assume that the operating point of the TIA is chosen such that saturation effects can be neglected. It is customary to consider current signals (and corresponding noise currents) at the receiver side. In this context, $I_{\mathsf{ref,rx}}$ denotes the receiver-sided reference current and a_{rx} a suitable scaling factor. Based on the received signal $s_{\mathsf{rx}}(t)$, the transmitted information bits $\hat{d}[n]$ can finally be recovered. Altogether, we have

$$s_{\mathsf{rx}}(t) := \Upsilon(d,\lambda) \cdot s(t), \tag{1}$$

where

$$\Upsilon(d,\lambda) := a_{\mathsf{rx}}/I_{\mathsf{ref,rx}} \cdot r_{\mathsf{OE}}(\lambda) \cdot L_0(d,\lambda) \cdot \alpha_{\mathsf{EO}} \cdot a_{\mathsf{tx}} \cdot I_{\mathsf{ref}} \tag{2}$$

denotes the overall proportionality factor between transmitter and receiver in the signal domain. In the presence of a (narrowband) optical receive filter, (1) becomes

$$s_{\mathsf{rx}}(t) := \Upsilon(d,\lambda) \cdot \xi \cdot s(t), \tag{3}$$

where $\xi < 1$ denotes the associated power attenuation factor [3].

Given a desired illumination level at the location of the VLC receiver (e.g. in terms of a specified illuminance of X lux), the DC component $I_{\mathsf{DC,f}}$ needs to be adjusted accordingly. Standard M-ary PPM uses a fixed duty cycle and transmits $\log_2(M)$ bits during one symbol duration T_{s}, by sending a pulse of length $T_{\mathsf{p}} = T_{\mathsf{s}}/M$ within one of the available time slots $[mT_{\mathsf{p}},\ (m+1)T_{\mathsf{p}}]$, where $m \in \{0, 1, \ldots, M-1\}$ denotes the current M-PPM symbol. The duty cycle is thus $\delta = 1/M$. Given the desired DC level and the dynamic range of the LED, the amplitude of the M-PPM signal $s(t)$ needs to be adjusted according to $\hat{A}_M = M \cdot I_{\mathsf{DC,f}}/(a_{\mathsf{tx}} \cdot I_{\mathsf{ref}})$. The corresponding photo current at the receiver has an amplitude of $\hat{I}_{\mathsf{p}} = r_{\mathsf{OE}}(\lambda) \cdot L_0(d,\lambda) \cdot \alpha_{\mathsf{EO}} \cdot M \cdot I_{\mathsf{DC,f}}/2$. In the following, let E'_{s} denote the received energy per M-PPM pulse in the electrical domain (in A^2 s), which can be expressed as $E'_{\mathsf{s}} = T_{\mathsf{p}} \cdot \hat{I}_{\mathsf{p}}^2$. Correspondingly, the received symbol energy E'_{s} is directly determined by the DC component $I_{\mathsf{DC,f}}$ of the LED driver current ($E'_{\mathsf{s}} \propto I_{\mathsf{DC,f}}^2$), and thus by the desired illumination level X.

The receiver noise is composed of thermal noise and shot noise [2, Ch. 3.7]. The latter is generally signal-dependent and non-Gaussian [16]. Throughout this paper, we assume that ambient light sources are present. In this case, the overall receiver noise can be regarded as signal-independent and Gaussian-distributed [17]. In the following, let N'_0 denote the single-sided noise power spectral density of the overall receiver noise in the electrical domain (in A^2/Hz). The signal-to-noise ratio (SNR) at the receiver is thus defined as

$$\gamma_{\mathsf{s}} := \frac{E'_{\mathsf{s}}}{N'_0} = \frac{E_{\mathsf{s}}}{N_0}, \tag{4}$$

where $E_{\mathsf{s}} := E'_{\mathsf{s}}/(1\ \mathrm{A}^2\mathrm{s})$ and $N_0 := N'_0/(1\ \mathrm{A}^2/\mathrm{Hz})$ denote the corresponding quantities in the signal domain. Throughout, we assume simple baseband processing in the electrical domain without any additional mixing steps. The electrical signal spectrum is thus centered around $f = 0$ Hz. Stated bandwidths refer to the one-sided 3-dB bandwidth.

A. Scenarios for Heterogeneous Optical Receivers

Without an optical blue filter at the receiver, the VLC link is dominated by the relatively slow rise and fall times of the phosphor (YAG) coating. As the white-light LED is directly modulated by an alternating current $i_{\mathsf{f}}(t)$, the corresponding frequency response in the electrical domain may be modeled by a first-order low-pass filter [18, Ch. 24.1], i.e., $H_{\mathsf{LED,YAG}}(f) \approx (1 + j \cdot f/W_{\mathsf{YAG}})^{-1}$. Here, W_{YAG} denotes the 3-dB bandwidth of the phosphor, which is on the order of a few megahertz in practice [2, Ch. 3.2] (typically 1...4 MHz). The corresponding impulse response reflects the slow response time of the phosphor and is given by $h_{\mathsf{LED,YAG}}(t) = 1/\tau_{\mathsf{YAG}} \cdot \exp(-t/\tau_{\mathsf{YAG}}) \cdot \Theta(t)$, where $\tau_{\mathsf{YAG}} = 1/(2\pi \cdot W_{\mathsf{YAG}})$. The core LED, on the other hand, offers significantly higher switching rates and thus a higher 3-dB

bandwidth W_{B}, typically $\geq$ 20 MHz [8]. Correspondingly, if an optical blue filter is employed at the receiver, which filters out a large fraction of the phosphor spectrum, the frequency response of the LED may be approximated as $H_{\mathsf{LED,B}}(f) \approx (1 + j \cdot f/W_{\mathsf{B}})^{-1}$ with impulse response $h_{\mathsf{LED,B}}(t) = 1/\tau_{\mathsf{B}} \cdot \exp(-t/\tau_{\mathsf{B}}) \cdot \Theta(t)$, where $\tau_{\mathsf{B}} = 1/(2\pi \cdot W_{\mathsf{B}})$.

As discussed in [9], if the received SNR is sufficiently large, the 3-dB bandwidth W_{YAG} may actually not be the limiting factor for data transmission, even without optical blue filter at the receiver. However, when exceeding W_{YAG}, one encounters a non-flat frequency response in the electrical domain, which requires corresponding equalization techniques at the receiver. For pulse-based modulation schemes, this typically adds significant computational complexity at the receiver side. In order to fully exploit the potential of PPM to offer a simplistic VLC transmission scheme, equalization at the receiver should therefore be avoided. By employing an optical blue filter at the receiver, symbol rates may be adjusted to W_{B} rather than to W_{YAG}, while ISI effects can widely be avoided. Thus, receiver complexity is moved from the digital domain to the optical domain. Yet, this solution is only feasible, if the SNR at the receiver is sufficiently high, due to the power attenuation factor ξ of the optical filter. As an example, we conducted light simulations for a simple office setup (the details are found in Appendix A). Without dimming, we found that very high SNR values in excess of 60 dB are attained at the receiver, even if an optical blue filter is employed. Furthermore, the coverage area of a single LED tends to be quite large. Correspondingly, it is realistic that more than one VLC user may be served by the same LED.

Our objective is to support the simple receiver and the sophisticated receiver with optical blue filter *simultaneously*, using a single LED-based transmitter. To this end, we propose a corresponding pairing of users[2] and seek to exploit the comfortable SNR margin. At the same time, there should remain room for dimming (e.g., in daylight scenarios), to avoid unnecessary energy consumption and possible dazzle effects.

B. Design Considerations for Nested PPM

With regard to a simplistic transmitter and receiver structure, we propose PPM as a basic building block to accommodate both users within a common waveform. The basic idea of nPPM is to use an M_1-PPM scheme for the user without optical blue filter – in the sequel denoted as "slow receiver" – and to embed a substructure within the M_1-PPM signal, which is intended for transmitting data to the sophisticated ("fast") receiver with optical blue filter.[3] As such, the pulse length of the M_1-PPM scheme will be chosen as $T_{\mathsf{p},1} = 1/(2\,W_{\mathsf{YAG}})$, and the symbol duration is given by $T_{\mathsf{s},1} = M_1 \cdot T_{\mathsf{p},1}$. The embedded substructure for the fast receiver then needs to comply with the electrical bandwidth W_{B} of the blue core LED. In contrast to coherent modulation schemes such as phase-shift keying (PSK) or quadrature-amplitude modulation (QAM), the bandwidth efficiency of M-PPM does not improve with growing M, since the number of required time slots increases accordingly. Yet, increasing M leads to a higher power efficiency in terms of energy per bit, which is also contrary to PSK and QAM [19, Ch. 4.4]. Correspondingly, higher-order PPM schemes are mainly relevant for energy-constrained data transmission applications. We therefore propose to employ a cardinality of $M_1 = 2$ for the slow receiver.

Let $F_{\mathsf{b}} := W_{\mathsf{B}}/W_{\mathsf{YAG}}$ denote the bandwidth factor between the fast and the slow receiver. Since we are mainly interested in bandwidth factors which are powers of two, we define

$$\bar{F}_{\mathsf{b}} := 2^{\lfloor \log_2(F_{\mathsf{b}}) \rfloor} \tag{5}$$

and consider values of $\bar{F}_{\mathsf{b}} \leq 16$ in the sequel. Correspondingly, within the symbol interval $T_{\mathsf{s},1}$ of the slow receiver, there are altogether $M_1 \bar{F}_{\mathsf{b}} = 2\bar{F}_{\mathsf{b}}$ time slots of length $T_{\mathsf{p},2} = 1/(2\,W_{\mathsf{B}})$ available for transmitting dedicated bits to the fast receiver.

Proposed Nested PPM scheme: We propose to use a single time slot of length $T_{\mathsf{p},2}$ to convey information bits to the fast receiver, by placing either an active pulse $\sqrt{E_{\mathsf{s}}} \cdot \mathrm{rect}(t/T_{\mathsf{p},2})$ within the inactive pulse interval of the outer PPM scheme or an inverted pulse $-\sqrt{E_{\mathsf{s}}} \cdot \mathrm{rect}(t/T_{\mathsf{p},2})$ within the active pulse interval of the outer PPM scheme. By this means, an "inner" $2\bar{F}_{\mathsf{b}}$-PPM scheme for the fast receiver is established. The proposed nPPM scheme is illustrated in Fig. 2. Note that the slow receiver will not be able to reliably detect the short pulses (or gaps) intended for the fast receiver, since the available time resolution associated with the electrical bandwidth W_{YAG} is not sufficient. The fast receiver, however, will be able to resolve *both* the outer 2-PPM pulses *and* the embedded $2\bar{F}_{\mathsf{b}}$-PPM structure. A rate analysis shows that our proposed nPPM scheme improves upon conventional time sharing [20, Ch. 6.2], when the bit rate of the slow receiver is supposed to be retained. In particular, we consider transmitted bit rates $\bar{r}$ in terms of bits per symbol interval $T_{\mathsf{s},1}$ of the slow receiver. The asymptotic information rate for $\gamma_{\mathsf{s}} \to \infty$ is given by

$$R = W_{\mathsf{YAG}} \cdot \bar{r} \ \ [\mathrm{bit/s}] \tag{6}$$

and depends on the particular electrical bandwidth W_{YAG} of the phosphor. Correspondingly, $\bar{r}$ may be interpreted as the spectral efficiency in bit/s/Hz. In the case of a single user with slow receiver, the transmitted bit rate is given by $\bar{r}_{\mathsf{YAG,su}} = 1$. A single user with fast receiver can attain a transmitted bit rate of $\bar{r}_{\mathsf{B,su}} = \bar{F}_{\mathsf{b}}$ by employing a 2-PPM scheme. In a multicast setting, any rate pair

$$(\bar{r}_{\mathsf{YAG}}, \bar{r}_{\mathsf{B}}) = ((1 - t_{\mathsf{s}}) \cdot \bar{r}_{\mathsf{YAG,su}}, t_{\mathsf{s}} \cdot \bar{r}_{\mathsf{B,su}}) \tag{7}$$

($t_{\mathsf{s}} \in [0, 1]$) is feasible for the two users via time sharing [20, Ch. 6.2], as illustrated in Fig. 3. Our proposed nPPM scheme is able to maintain the bit rate of the slow receiver, while still offering a transmitted bit rate of $\log_2(2\bar{F}_{\mathsf{b}})$ for the fast receiver. It therefore outperforms conventional time sharing in this regime. In a broadcast scenario, a common message might be transmitted to the two users (in terms of the bits $d_1[n]$), so that the bits $d_1[n]$ *and* $d_2[n]$ are intended for the fast receiver. Examples include

[2] If only a single user is present, the VLC system can simply switch to conventional PPM with symbol duration adjusted to W_{YAG} or W_{B}, while multiple users of one kind may be accommodated via time sharing.

[3] Within the scope of this paper, the notions of "fast" and "slow" receiver refer only to the fact, whether the PD employs a dedicated optical filter or not, and do not refer to any absolute measure.

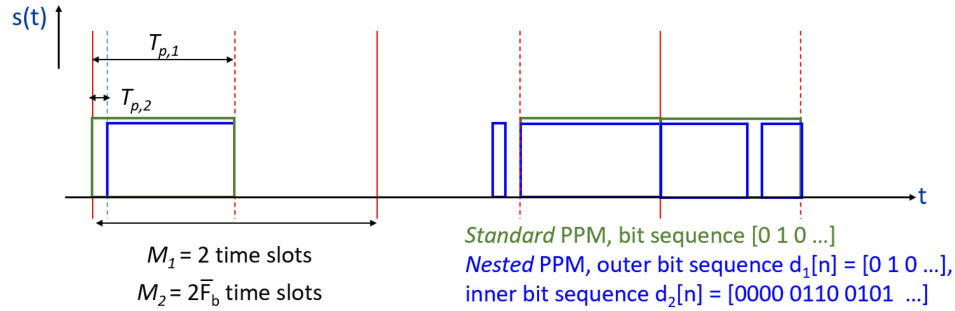

Fig. 2. Proposed nested PPM (nPPM) scheme for the example $\bar{F}_b = 8$.

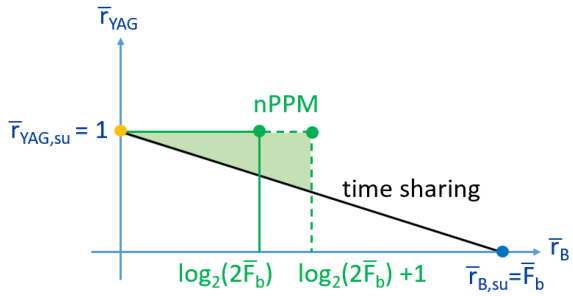

Fig. 3. Rate region $(\bar{r}_{YAG}, \bar{r}_B)$ for the heterogeneous receivers. The proposed nPPM scheme is marked in green (solid lines: multicast setting, dashed lines: broadcast setting).

video streaming or image transmission employing hierarchical bit mapping, where the slow receiver obtains a low image resolution (based on the bits $d_1[n]$), whereas the fast receiver obtains a higher image resolution. In this case, the proposed nPPM scheme attains a transmitted bit rate of $\bar{r} = \log_2(2\bar{F}_b) + 1$ for the fast receiver, due to the extra bit from the outer 2-PPM scheme.

Note that the simplistic transmitter structure of a standard PPM scheme is largely retained for the proposed nPPM scheme, since in essence only two software-controlled switches with elementary logic are required to generate the outer 2-PPM pulses and the embedded substructure for the inner PPM scheme. The same is true for the receiver side, as symbol detection still relies on basic I&D operations and some rudimentary signal operations (details can be found in Appendix B). Next, we turn our attention to the resulting error performance of our proposed nPPM scheme.

III. Error Performance Analysis for Nested PPM

The symbol-error probability (SEP) of the outer and the inner PPM scheme can be derived in semi-closed form providing integral expressions, which can be evaluated by means of numerical integration. For our analysis, we assume a non-dispersive additive white Gaussian noise (AWGN) channel and neglect any ISI effects caused by non-ideal filtering (these aspects will be addressed in Section IV). Our SEP results thus serve as upper performance bounds. To allow for a general comparison between the fast and the slow receiver, the power attenuation factor ξ of the optical filter is disregarded in our analysis, as it depends on the optical spectrum of the employed white-light LED as well as on the type of optical filter. Yet, it was included in our numerical examples in Appendix A regarding the available received SNR. The outer 2-PPM scheme for the slow receiver and the embedded inner PPM scheme for the fast receiver constitute a hierarchical modulation scheme. For symbol detection, the slow receiver employs a matched filter in the form of an I&D operation tailored to the pulse length $T_{p,1}$ of the outer 2-PPM scheme. Assuming perfect time synchronization at symbol level, maximum-likelihood (ML) symbol detection is then performed by selecting the pulse interval with the larger integration result. The fast receiver first detects the outer 2-PPM symbol using the identical steps as the slow receiver. To detect the embedded inner PPM symbol, it then employs an I&D operation tailored to the pulse length $T_{p,2}$. This leads to error propagation, if the symbol detection for the outer 2-PPM scheme is not correct. This effect is well-known from layered modulation schemes with successive interference cancellation (SIC) at the receiver (e.g., [21], [22]). However, in our approach the detected signal of the first user is not subtracted from the received signal (as done in SIC), but merely serves as a starting point for the detection of the embedded PPM symbols for the second user (the details are found in Appendix B). The resulting SEP for the slow receiver is given by (23), and the SEP expressions for the fast receiver are given by (27) and (28) for the multicast and the broadcast case, respectively.

Fig. 4 illustrates the performance of the proposed nPPM scheme for selected examples. The derived SEP expressions are validated by means of corresponding Monte-Carlo computer simulations conducted over 10^6 blocks of 10 random PPM symbols each. The analytical results are represented by lines, and corresponding simulation results are marked by circles (○). As can be seen, analytical and simulation results are virtually identical. For the inner PPM scheme (fast receiver) two different bandwidth factors are compared, namely $\bar{F}_b = 8$ (solid lines) and $\bar{F}_b = 16$ (dashed lines). Reference curves for conventional PPM are also included for the slow receiver and for the fast receiver with $\bar{F}_b = 8$ (dotted lines). In particular, the conventional 2-PPM curve for the slow receiver defines the reference for the received SNR γ_s. Correspondingly, the conventional PPM curve for the fast receiver exhibits an SNR shift of $10\log_{10}(\bar{F}_b)$ dB (i.e., 9.03 dB for $\bar{F}_b = 8$), since the pulse length employed by

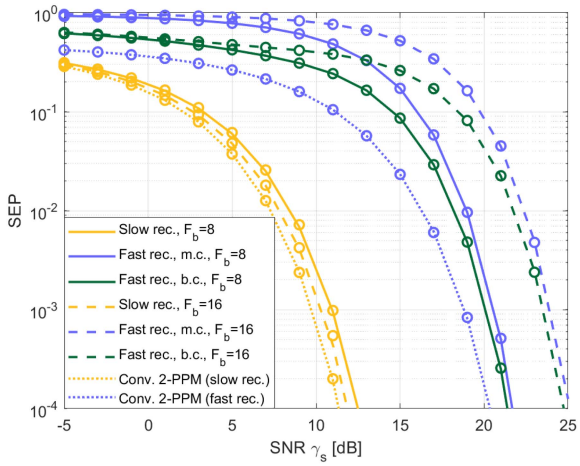

Fig. 4. SEP performance of the proposed nPPM scheme for the AWGN case. For the inner PPM scheme (fast receiver), bandwidth factors of $\bar{F}_\mathsf{b} = 8$ (solid lines) and $\bar{F}_\mathsf{b} = 16$ (dashed lines) were evaluated, both for a multicast (m.c.) and a broadcast (b.c.) scenario. Reference curves for conventional (conv.) 2-PPM are also included for the slow receiver (rec.) and the fast receiver (rec.) for $\bar{F}_\mathsf{b} = 8$ (dotted lines).

the inner PPM scheme is reduced by a factor of $1/\bar{F}_\mathsf{b}$, entailing a corresponding energy loss.

The SEP performance of the outer PPM scheme (slow receiver, yellow lines) is very close to that of conventional 2-PPM, while a small SNR loss of $20\log_{10}((\bar{F}_\mathsf{b}-1)/\bar{F}_\mathsf{b})$ dB is observed (i.e., 1.16 dB for $\bar{F}_\mathsf{b} = 8$ and 0.56 dB for $\bar{F}_\mathsf{b} = 16$), as predicted by the analytical results. For the inner PPM scheme (fast user) a small additional performance loss is observed in the multicast scenario compared to conventional PPM (about 1.4 dB for $\bar{F}_\mathsf{b} = 8$, blue line), which is due to the error propagation effect. The SEP performance for the broadcast case (dark green lines) is slightly better than for the multicast case, because the 2-PPM symbols shared with the slow receiver have a lower error probability, which reduces the (average) SEP compared to the multicast case. With regard to the discussion in Section II-A and Appendix A, the (combined) SNR loss for the fast receiver seems affordable, however, even in the case of dimming. For example, for the scenario considered in Fig. 2, an SNR value of $\gamma_\mathsf{s} = 66.7$ dB was obtained for the center of the office desk, considering the case $M = 2$ in the presence of an optical blue filter. Correspondingly, given an outer 2-PPM scheme, in order to maintain an SNR value of, say $\gamma_\mathsf{s} = 25$ dB, so as to achieve a SEP smaller than 10^{-4} for the inner PPM scheme, there is still an SNR margin of 41.7 dB. This allows for a reduction of the illuminance E_V below 1% (in this case below 3.2 lx), which corresponds to a perceived light intensity of 10% [2, Ch. 2.6]). If the location of the receiver is moved away from the center of the office desk, the illuminance values at the receiver are reduced due to a combination of an increased distance and a reduced luminous intensity, caused by the restricted field of view of the luminaire. Yet, even in the corner of the room the resulting SNR margin is still on the order of 25 dB.

Note that for the slow receiver the bit-error probability (BEP) is the same as the above SEP, since we employ a binary PPM scheme throughout ($M_1 = 2$). For the fast receiver it was found that the BEP in the multicast scenario can be tightly approximated by $\mathrm{BEP} \approx M_2/2 \cdot \mathrm{SEP}/(M_2 - 1)$, which is known to be an exact BEP expression in the case of standard M_2-PPM [19, Ch. 4.4].

IV. Comprehensive End-to-End VLC System Model

To derive our SEP bounds in Section III, we have so far disregarded any ISI effects. However, in order to obtain realistic predictions of symbol-error-rates (SERs) achievable in practice, we need to extend the signal model (1) accordingly. In the following, we include special characteristics of phosphorescent white-light LEDs and tailor the signal model to our discussed receiver types with and without optical blue filter. The following assumptions are made:

- To model the electronic properties of the LED, we adopt the first-order low-pass filter models $H_{\mathsf{LED,B}}(f)$ and $H_{\mathsf{LED,YAG}}(f)$ for the case with and without optical blue filter, respectively (cf. Section II-A).
- Throughout, we focus on a line-of-sight (LoS) scenario and assume a non-dispersive AWGN channel for the VLC link (i.e., $C(f) = 1$, cf. Fig. 1). An extension to non-LoS scenarios is straightforward, however [23].
- Typically, the electrical bandwidth of the PD (and the subsequent TIA) is significantly larger than the bandwidth of the LED (e.g. ≥ 100 MHz [1, Ch. 2.4]), so that we retain the assumption $H_{\mathsf{PD}}(f) = 1$ in the sequel.
- In phosphorescent white-light LEDs, typically only a certain fraction of the blue-light photons emitted by the core LED is absorbed by the phosphor and converted to longer wavelengths (by a combination of nonradiative decay to lower energy levels and luminescent emission [24, Ch. 3.17]). Correspondingly, emitted light spectra contain a distinct peak in the blue region [2, Ch. 2.4]. To account for this effect, we introduce a relative power weighting factor $0 \leq \Delta < 1$ for the blue spectrum part, while the spectrum part generated by the phosphor is associated with the factor $1 - \Delta$. In the presence of an optical blue filter at the receiver, the power weighting factor Δ is absorbed by the power attenuation factor ξ, which also includes the transmittance of the blue filter. For the receiver without optical blue filter, we assume for simplicity that the PD does not employ any integrated optical filter.
- Finally, there is a slight overlap between the optical spectra of the phosphor and the blue core LED [24, Ch. 3.17]. Correspondingly, an optical blue filter at the receiver will not be able to remove the contribution of the phosphor entirely. We account for this effect by introducing a corresponding interference factor $\varepsilon_{\mathsf{YAG}} \geq 0$.

Based on the above considerations, we devise the following end-to-end (E2E) signal models for the case with and without optical blue filter at the receiver:

Signal Model Without Optical Blue Filter: The E2E signal model for the case without optical receiver filter (slow receiver) is given by

$$s_{\mathsf{rx,s}}(t) = \Upsilon(d, \lambda_{\mathsf{YAG}}) \cdot \Big((1-\Delta) \cdot h_{\mathsf{LED,YAG}}(t) * s(t)$$

$$+\ \Delta \cdot \frac{r_{\mathsf{OE}}(\lambda_{\mathsf{B}})}{r_{\mathsf{OE}}(\lambda_{\mathsf{YAG}})} \cdot h_{\mathsf{LED,B}}(t) * s(t)\Big), \tag{8}$$

where λ_{YAG} represents the effective center wavelength of the phosphor (e.g., $\lambda_{\mathsf{YAG}} \approx 600$ nm [2, Ch. 2.4]) and λ_{B} the wavelength of the blue LED. Note that (8) includes the filter effects related to the electrical properties of the phosphor ($h_{\mathsf{LED,YAG}}(t)$) and the blue LED ($h_{\mathsf{LED,B}}(t)$). Furthermore, the second term in (8) represents an interference term caused by the blue spectrum part, which can not be resolved by the slow receiver, as the subsequent I&D operation is tailored to the small electrical bandwidth W_{YAG} of the phosphor. The interference term is limited by the factor $\Delta < 1$. Furthermore, the responsivity of the PD in the blue spectrum part is usually smaller than for longer wavelengths, i.e., $r_{\mathsf{OE}}(\lambda_{\mathsf{B}}) < r_{\mathsf{OE}}(\lambda_{\mathsf{YAG}})$ [1, Ch. 2.4.1].

Signal Model With Optical Blue Filter: The corresponding E2E signal model for the case with optical blue filter (fast receiver) is given by

$$s_{\mathsf{rx,f}}(t) = \Upsilon(d, \lambda_{\mathsf{B}}) \cdot \Big(\xi \cdot h_{\mathsf{LED,B}}(t) * s(t) + \varepsilon_{\mathsf{YAG}} \cdot \frac{r_{\mathsf{OE}}(\lambda_{\mathsf{YAG}})}{r_{\mathsf{OE}}(\lambda_{\mathsf{B}})} \cdot h_{\mathsf{LED,YAG}}(t) * s(t)\Big). \tag{9}$$

The second term in (9) represents an interference term caused by the phosphor spectrum part, which is limited by the factor $\varepsilon_{\mathsf{YAG}}$. It is mainly relevant for detecting the inner PPM scheme, for which the subsequent I&D operation is tailored to the larger electrical bandwidth W_{B} of the blue core LED.

In the following, we compare the numerical performance results obtained on the basis of the above E2E signal models with the performance bounds derived in Section III. To allow for a direct comparison and to highlight the influence of the LED frequency responses as well as the interference terms in (8) and (9), we disregard the power attenuation factor ξ for the presented SER results (as earlier). Note that the proportionality factors $\Upsilon(d, \lambda_{\mathsf{YAG}})$ and $\Upsilon(d, \lambda_{\mathsf{B}})$ affect the desired and the interference part of the received signals equally and are therefore normalized to one for simplicity. For the remaining parameters, the following values were assumed: $\Delta = 0.166$ [3], $r_{\mathsf{OE}}(\lambda_{\mathsf{B}}) = 0.28$ A/W, $r_{\mathsf{OE}}(\lambda_{\mathsf{YAG}}) = 0.42$ A/W [25], $\varepsilon_{\mathsf{YAG}} = 0.041$. The assumed value of Δ applies for the Solo Slim luminaire employed earlier in our numerical examples in Section II-A and Appendix A. The value for $\varepsilon_{\mathsf{YAG}}$ was estimated based on corresponding spectral measurements from an internal report provided by Regent Lighting.

Fig. 5 displays two example received signals for the nPPM scheme after the I&D operation according to the signal model (8)/(9). For the transmitted signals $s(t)$ (represented by the black lines), the parameter $\bar{F}_{\mathsf{b}} = 8$ was chosen. The start time t_0 of the I&D operation (14), cf. Appendix B, was optimized numerically, assuming ideal rectangular transmit pulses and taking the first-order low-pass behavior of the blue core LED and the phosphor into account. Considering a single transmitted pulse of length $T_{\mathsf{p},1}$ for the outer PPM scheme, the received signal energy $E_{\mathsf{s}}(t_0)$ is maximized for

$$t_0 \approx kT_{\mathsf{s},1} + mT_{\mathsf{p},1} - 0.286 \cdot T_{\mathsf{p},1}, \tag{10}$$

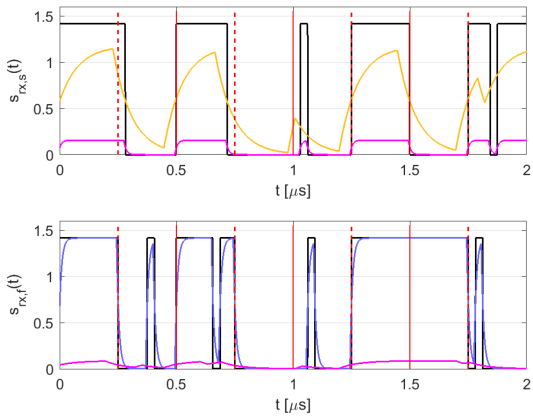

Fig. 5. Example receive signals for nPPM ($\bar{F}_{\mathsf{b}} = 8$) after the I&D operation according to the signal model (8)/(9): Slow receiver without optical blue filter (top), fast receiver with optical blue filter (bottom).

whereas the last term was $-T_{\mathsf{p},1}/2$ in the AWGN case. Since there is a fixed relation between the employed pulse length and the time constant τ of the associated first-order low-pass filter model, the offset factor -0.286 is also optimal for the inner PPM scheme (and is applied to $T_{\mathsf{p},2}$ in this case).[4] At the top of Fig. 5, the received signal of the slow receiver without optical blue filter is shown, where the yellow line represents the desired signal part and the magenta line the interference term in (8). The electrical bandwidth W_{YAG} of the phosphor was assumed to be 2 MHz. The dashed vertical lines represent the employed pulse duration $T_{\mathsf{p},1}$ and the solid vertical lines the corresponding symbol duration of the outer PPM scheme. The (asymptotic) information rate for the slow receiver according to (6) is given by 2 Mb/s. The scalings of the desired signal part and the interference term are associated with the factors $(1 - \Delta)$ and $\Delta \cdot r_{\mathsf{OE}}(\lambda_{\mathsf{B}})/r_{\mathsf{OE}}(\lambda_{\mathsf{YAG}})$, respectively. As expected, the slow receiver will not be able to resolve the embedded inner PPM signal intended for the fast receiver. Furthermore, note that signal artifacts from the blue core LED do not really constitute a harmful interference term. This is because the slow receiver will capture the "envelope" of the underlying signal $h_{\mathsf{LED,B}}(t) * s(t)$, which actually contributes constructively to the detection of the outer PPM signal. At the bottom of Fig. 5, the received signal of the fast receiver with optical blue filter is shown. The desired signal part is represented by the blue line and the interference term in (9) by the magenta line. As expected, the fast receiver is able to follow the fast signal changes of the embedded PPM signal. The interference term will not contribute constructively to the detection of the embedded PPM signal, however. Yet, its impact will be limited due to the small value of $\varepsilon_{\mathsf{YAG}}$.

For the corresponding numerical SER results presented in the following, the desired parts of the received signals were normalized to a common symbol energy E_{s}, and the interference parts were scaled accordingly. Fig. 6 (top) shows the resulting SER performance for the slow receiver, both w.r.t. the outer PPM

[4] An improved SER performance could be achieved by employing a matched filter tailored to the low-pass filtered received pulse shape. For the sake of a simple receiver, we have retained the basic I&D scheme with constant gain over the pulse duration and only optimized the start time t_0 of the integration.

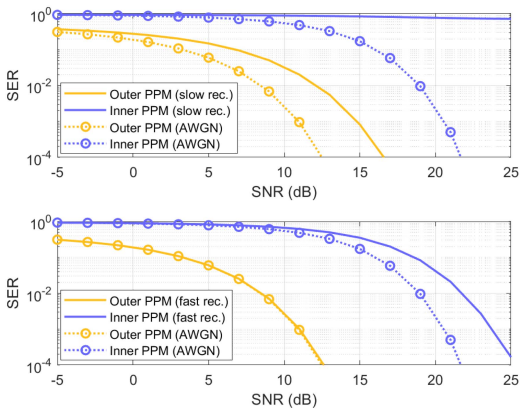

Fig. 6. SER performance for nPPM ($\bar{F}_\mathrm{b} = 8$; multicast scenario) for (i) the slow receiver (rec.) without optical blue filter (top) according to the signal model (8), regarding its own data ("Outer PPM", yellow line) and the data intended for the fast receiver ("Inner PPM", blue line) and (ii) the fast receiver with optical blue filter (bottom) according to the signal model (9), regarding its own data ("Inner PPM", blue line) and the data intended for the slow receiver ("Outer PPM", yellow line). The dotted curves represent the performance bounds derived for the AWGN case.

signal (intended for this user, yellow curve) and the embedded inner PPM signal (intended for a user with optical blue filter, blue curve). The performance bounds derived in Section III for the AWGN case are included as a reference (dotted lines). As can be seen, the performance degradation for the outer PPM signal compared to the AWGN case is approximately 4 dB. This is attributed to the scaling factor $(1 - \Delta)$ and ISI effects caused by the frequency response and limited electrical bandwidth of the phosphor. The interference term indeed contributes constructively to the I&D detection step for the outer PPM signal, as a performance improvement of about 1 dB is observed compared to the case when the interference term is set to zero (not depicted). As expected, the slow receiver is not able to generate reliable symbol decisions for the inner PPM scheme, as the corresponding SER curve exhibits a high error floor. Fig. 6 (bottom) shows the corresponding SER performance for the fast receiver. As can be seen, the fast receiver is able to detect the outer and the inner PPM symbols (this is required for the employed hierarchical demodulation and also enables the concept of a common message in the broadcast case). In particular, the ISI effect for detection of the outer PPM symbols (yellow curve) is negligible, due to the increased electrical bandwidth of the fast receiver (bandwidth factor $\bar{F}_\mathrm{b}$). For the inner PPM signal (blue curve), a performance degradation of about 3.1 dB is observed compared to the AWGN case (at a SER of 10^{-3}), which is attributed to error propagation and ISI effects (caused by the frequency response of the blue core LED). In light of the discussion in Section II-A and Appendix A this still seems feasible, due to the high SNR margin in many practical settings.

V. Possible Extensions

Within the scope of this paper, we have focused on PPM as a basic building block for our hierarchical modulation scheme. There are a couple of interesting variations and extensions for future consideration:

- The proposed nPPM scheme could directly be extended to Variable PPM (VPPM) [5] as a basic building block, in order to provide an additional illumination control in the signal domain, e.g., for peak-power limited VLC systems: While with standard PPM illumination is controlled by adapting the amplitude $\hat{A}_M$ of the PPM signal, VPPM employs a variable duty cycle $\delta = v/M$.
- In order to enhance data rates, a combination of PPM and Q-ary pulse-amplitude modulation (PAM) could be employed for the outer and/or the inner modulation scheme. To this end, the active PPM pulses are combined with Q possible amplitude levels, which increases the number of transmitted bits per symbol duration by $\log_2(Q)$ bits (at the expense of a higher required SNR).
- Another interesting extension could be to simultaneously support $K > 1$ slow receivers and/or $K' > 1$ fast receivers, via a combination of time-sharing and PPM/Q-PAM modulation with user-dependent bit mapping.

With any of these extensions, the simplistic transmitter and receiver structure of nPPM will largely be retained.

VI. Conclusion

We have considered VLC using phosphorescent white-light LEDs and two different receiver types – a "slow" receiver for moderate data rate requirements and a "fast" receiver for higher data rate requirements equipped with an optical blue filter. With the goal to accommodate both receiver types simultaneously using a single LED-based transmitter, we have proposed a hierarchical "nested" PPM scheme, which improves upon conventional time sharing, when the bit rate of the slow receiver is supposed to be retained. An analysis of the available SNR at the receiver for a practical setting combined with analytical and simulated error performance results has corroborated the feasibility of our approach. Finally, we have devised an E2E VLC signal model, which included the electrical properties of the LED and interference effects associated with the optical filtering. We have shown that the influence of the underlying filter operations on the resulting error performance for the slow and the fast receiver is moderate, which underlines the practicability of the proposed nPPM scheme.

Due to its simplicity regarding the transmitter and receiver structure, the proposed nPPM scheme may be relevant for future mass-market VLC deployments as well as for proprietary solutions. For future work, extensions of the presented ideas to multiple slow and/or multiple fast receivers as well as to other hierarchical modulation schemes will be of interest, along with corresponding practical realizations based on low-cost software and hardware components.

Appendix

A. Light Simulation Example for an Office Setup

To assess the SNR margin available in a practical setting, we conducted example simulations for a simple office

TABLE I
PARAMETER VALUES EMPLOYED FOR SNR EVALUATION

Parameter	Description	Value
$r_{\mathrm{OE}}(\lambda_{\mathrm{B}})$	Responsivity of PD (at wavelength λ_{B})	0.28 A/W
λ_{B}	Center wavelength of blue core LED	450 nm
ξ	Power attenuation factor of optical receive filter (desired signal)	0.149
A_{meas}	PD area of VLC receiver	100 mm^2
$V(\lambda_{\mathrm{B}})$	Eye sensitivity curve (at wavelength λ_{B})	0.04
ξ_{d}	Power attenuation factor of optical receive filter (daylight)	0.108
T_{a}	Absolute temperature	293.15 K
R_{F}	Feedback resistor TIA	10 kΩ
W_{MF}	Bandwidth of matched filter ($= W_{\mathrm{B}}$)	20 MHz

setup using the 3D light planning tool *ReluxDesktop* (Version 2020.2.5.0) [26]. The considered setup was the same as in [3] and is described there in detail. The key parameters are also summarized in Table I. The room dimensions were 5 m × 5 m × 3 m, and the room included a window of size 1.5 m × 1.5 m, admitting full daylight into the room. Further ambient light sources were not taken into account. At the center of the ceiling, a single Regent Solo Slim luminaire with a luminuous flux of 4350 lm was placed, and a desk with height 0.75 m was found directly underneath the luminaire. The light distribution curve (LDC) of the luminaire is documented in [3]. The resulting illuminance values were evaluated across the entire room for a reference plane at desk height. In particular, the contributions of the considered luminaire and the daylight were evaluated separately. The results are illustrated in Fig. 7. For the luminaire, an illuminance value of $E_{\mathrm{V}} = 319$ lux was measured at the center of the desk, while the daylight contributed an additional illuminance of $E_{\mathrm{V,d}} = 675$ lux.[5] The daylight was simulated using the CIE "clear sky with sun" model [28]. For scenarios with overclouding, the resulting illuminance value will be reduced accordingly.

Based on the simulated illuminance values E_{V} and $E_{\mathrm{V,d}}$, the received SNR γ_{s} at the center of the desk may be calculated along the lines of [3] (see also [2, Ch. 3.7]):

$$\gamma_{\mathrm{s}} \approx \frac{\kappa \cdot \left(\frac{r_{\mathrm{OE}}(\lambda_{\mathrm{B}}) \cdot \xi \cdot A_{\mathrm{meas}}}{683 \frac{\mathrm{lm}}{\mathrm{W}} \cdot V(\lambda_{\mathrm{B}})} \cdot E_{\mathrm{V}} \right)^2}{4 \cdot \left(\frac{e_0 \cdot r_{\mathrm{OE}}(\lambda_{\mathrm{B}}) \cdot \xi_{\mathrm{d}} \cdot A_{\mathrm{meas}}}{683 \frac{\mathrm{lm}}{\mathrm{W}} \cdot V(\lambda_{\mathrm{B}})} \cdot E_{\mathrm{V,d}} + \frac{2\, k_{\mathrm{B}} \cdot T_{\mathrm{a}}}{R_{\mathrm{F}}} \right) \cdot W_{\mathrm{MF}}}, \quad (11)$$

where we have included the power attenuation factors ξ, ξ_{d} for an optical blue filter at the receiver. Furthermore, κ denotes the shaping gain factor, which is $\kappa = M$ for M-PPM

[5]Note that the European norm DIN EN 12464-1 (2021-11) recommends illuminance values ≥ 500 lux for typical office work [27].

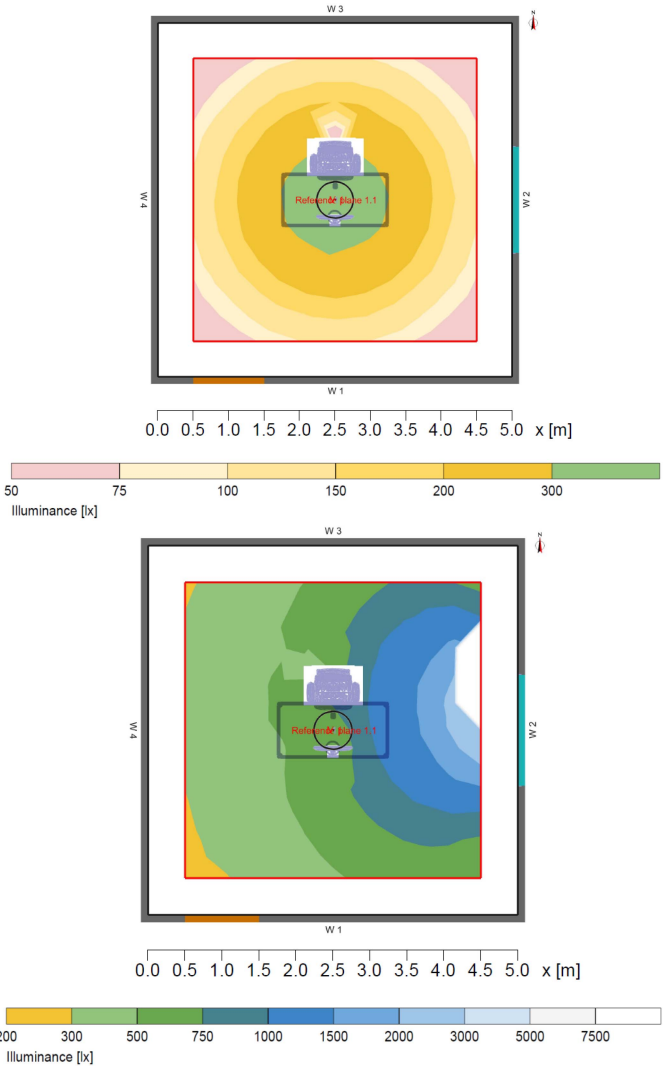

Fig. 7. Simulated illuminance values for the Regent Solo Slim luminaire (top) and the daylight admitted through the window (bottom).

signals, $e_0 = 1.602 \cdot 10^{-19}$ As denotes the elementary charge, and $k_{\mathrm{B}} = 1.38 \cdot 10^{-23}$ Ws/K is the Boltzmann constant. The remaining parameters are detailed in Table I. The first term in the denominator represents the shot noise, while the second term represents the thermal noise. Note that the "clear sky" model for the daylight serves as a worst-case scenario in this context, because it leads to the maximum shot noise level. The matched filter bandwidth is related to the pulse length T_{p} according to $W_{\mathrm{MF}} = 1/(2\,T_{\mathrm{p}})$. For further details, the interested reader is referred to [3]. The SNR values γ_{s} resulting for the parameter settings in Table I are illustrated in Fig. 8 for different cardinalities M of the PPM scheme, where the illuminance E_{V} was varied between 50 lx and 500 lx. The values obtained for the particular office scenario in Fig. 7 for the center of the desk are marked by the vertical dashed line. As can be seen, very high SNR values are attained, even if an optical blue filter is employed. Furthermore, when inspecting the top of Fig. 7, we find that the coverage area of the luminaire is relatively large,

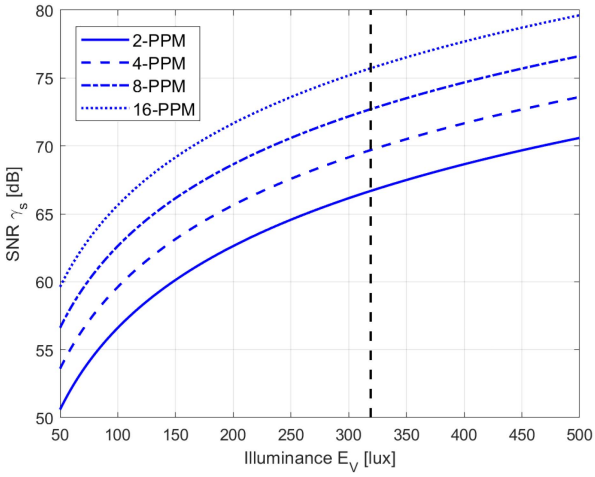

Fig. 8. Resulting SNR values γ_{s} for the example scenario, when employing an optical blue filter at the receiver.

although the LDC of the employed LED has a moderate width of about $\pm 40°$, judging from the half-power angle. For example, within a circle area of radius 1.75 m, the resulting illuminance values are still larger than 150 lx in this setting.

B. SEPs for Nested PPM in AWGN Channels

The SEP of conventional M-PPM with rectangular pulses and corresponding I&D receiver can be derived following the framework of optimal detection for orthogonal signals established in [19, Ch. 4.4], as M-PPM signals are mutually orthogonal and the I&D receiver provides the optimal (maximum-likelihood) detection strategy. The transmitted signal is given by

$$s_{\mathsf{PPM}}(t) := \sqrt{E_{\mathsf{s}}} \sum_{k=0}^{K-1} \mathrm{rect}\left(\frac{t - t_k + T_{\mathsf{p}}/2}{T_{\mathsf{p}}}\right), \tag{12}$$

where k denotes the discrete time index at symbol level, $t_k = t_k(m) := kT_{\mathsf{s}} + mT_{\mathsf{p}}$ denotes the start time of the k-th PPM pulse, and $m \in \{0, 1, \ldots, M-1\}$ is the current M-PPM symbol. Assuming a (normalized) non-dispersive optical channel, the received signal for K subsequent M-PPM symbols is given by

$$r(t) := s_{\mathsf{PPM}}(t) + w(t), \tag{13}$$

where $w(t) \sim \mathcal{N}(0, N_0/2)$ denotes the AWGN. The I&D operation for symbol hypothesis $\tilde{m} \in \{0, 1, \ldots, M-1\}$ reads

$$\frac{\sqrt{E_{\mathsf{s}}}}{T_{\mathsf{p}}} \int_{t_0}^{t_0+T_{\mathsf{p}}} r(t)\,\mathrm{d}t =: e_{\tilde{m}}, \tag{14}$$

where the integration start is given by $t_0 = t_k(\tilde{m}) - T_{\mathsf{p}}/2$ in the AWGN case with $t_k(\tilde{m}) := kT_{\mathsf{s}} + \tilde{m}T_{\mathsf{p}}$. Specifically, for the correct hypothesis $\tilde{m} = m$ we have $e_{\tilde{m}} = E_{\mathsf{s}}$ (disregarding noise). Following the framework in [19, Ch. 4.4], one obtains the SEP (or bit-error probability) expression $P_{\mathsf{s,e,2-PPM}} = P_{\mathsf{e}}(1,1)$ for $M = 2$ with $P_{\mathsf{e}}(Z, \nu)$ according to (15) shown at the bottom of this page. In the proposed nPPM scheme, an inner $2\bar{F}_{\mathsf{b}}$-PPM scheme is realized for the fast receiver, by either placing a gap of length $T_{\mathsf{p},2} = T_{\mathsf{p},1}/\bar{F}_{\mathsf{b}}$ within the outer 2-PPM pulse or by placing an short pulse of length $T_{\mathsf{p},2}$ within the unused time slot of the outer 2-PPM scheme. The received signal for the kth outer 2-PPM symbol is thus given by

$$r_{k,m_1,m_2}(t) := \sqrt{E_{\mathsf{s}}}\,\mathrm{rect}\left(\frac{t - t_k(m_1) + T_{\mathsf{p},1}/2}{T_{\mathsf{p},1}}\right) \pm \sqrt{E_{\mathsf{s}}}\,\mathrm{rect}\left(\frac{t - t_k(m_2) + T_{\mathsf{p},2}/2}{T_{\mathsf{p},2}}\right) + w(t). \tag{16}$$

If the PPM symbol m_2 of the inner scheme happens to fall in the interval of the active outer pulse, the sign of the inner pulse is negative, otherwise positive. The slow receiver does not have any means to detect the short gap or pulse introduced by the inner PPM scheme. For the fast receiver, the detection order is such that first the information bits $d_1[n]$ of the outer 2-PPM scheme are detected, and based on this, the information bits of the inner PPM scheme are detected in a second step. Correspondingly, we assume for both optical receiver types that the standard I&D operation (14) is employed for detecting the bits $d_1[n]$ of the outer 2-PPM scheme. If the PPM symbol of the inner scheme falls in the interval of the active outer pulse, one obtains

$$e_{\tilde{m}_1} = \begin{cases} \frac{\bar{F}_{\mathsf{b}}-1}{\bar{F}_{\mathsf{b}}} \cdot E_{\mathsf{s}} + \sqrt{E_{\mathsf{s}}} \cdot w_{k,m_1}, & \text{for } \tilde{m}_1 = m_1 \\ \sqrt{E_{\mathsf{s}}} \cdot w_{k,\tilde{m}_1}, & \text{for } \tilde{m}_1 \neq m_1 \end{cases}, \tag{17}$$

where $w_{k,m_1}, w_{k,\tilde{m}_1} \sim \mathcal{N}(0, N_0/2)$ are independent and identically distributed (i.i.d.) AWGN samples. The probability for correct detection of the outer 2-PPM symbol m_1 is thus associated with the event

$$\mathcal{E} = \left\{(\bar{F}_{\mathsf{b}} - 1)\sqrt{E_{\mathsf{s}}}/\bar{F}_{\mathsf{b}} + w_{k,m_1} > w_{k,\tilde{m}_1}\right\} \tag{18}$$

and may be written as

$$P_{\mathsf{b,c}} = \int_{-\infty}^{+\infty} P_{m_1}(w_{k,m_1}) \cdot p(w_{k,m_1}) \cdot \mathrm{d}w_{k,m_1}, \tag{19}$$

where

$$P_{m_1}(w_{k,m_1}) = 1 - \mathrm{Q}\left(\frac{(\bar{F}_{\mathsf{b}} - 1)\sqrt{E_{\mathsf{s}}}/\bar{F}_{\mathsf{b}} + w_{k,m_1}}{\sqrt{N_0/2}}\right) \tag{20}$$

and

$$p(w) := \frac{1}{\sqrt{\pi N_0}} \cdot \exp\left(-\frac{1}{2} \cdot \frac{w^2}{N_0/2}\right) \tag{21}$$

denotes the Gaussian probability density function. Employing the substitution

$$y := \sqrt{2}\left((\bar{F}_{\mathsf{b}} - 1)\sqrt{E_{\mathsf{s}}}/\bar{F}_{\mathsf{b}} + w_{k,m_1}\right)/\sqrt{N_0}, \tag{22}$$

$$P_{\mathsf{e}}(Z, \nu) = 1 - \frac{1}{\sqrt{2\pi}} \int_{-\infty}^{+\infty} [1 - \mathrm{Q}(y)]^{\nu} \cdot \exp\left(-\frac{1}{2}\left(y - Z\sqrt{2\gamma_{\mathsf{s}}}\right)^2\right) \cdot \mathrm{d}y \tag{15}$$

$$P_{\mathsf{s,e,nPPM-i}} = (1 - P_{\mathsf{s,e,nPPM-o}}) \cdot P_{\mathsf{e}}\left(1/\sqrt{\bar{F}_{\mathsf{b}}}, 2\bar{F}_{\mathsf{b}} - 1\right) + P_{\mathsf{s,e,nPPM-o}} \cdot P_{\mathsf{e}}\left(-1/\sqrt{\bar{F}_{\mathsf{b}}}, 2\bar{F}_{\mathsf{b}} - 1\right) \tag{27}$$

we arrive at $P_{\mathsf{b,c}} = 1 - P_{\mathsf{e}}((\bar{F}_{\mathsf{b}} - 1)/\bar{F}_{\mathsf{b}}, 1)$ with $P_{\mathsf{e}}(Z, \nu)$ according to (15). If the PPM symbol of the inner scheme falls in the unoccupied pulse interval of the outer 2-PPM scheme, the same probability $P_{\mathsf{b,c}}$ results. Altogether, we thus get the SEP expression

$$P_{\mathsf{s,e,nPPM-o}} = P_{\mathsf{e}}\left((\bar{F}_{\mathsf{b}} - 1)/\bar{F}_{\mathsf{b}}, 1\right) \tag{23}$$

for the outer 2-PPM scheme.

The fast receiver first needs to detect the symbol m_1 of the outer PPM scheme, before the inner PPM symbol m_2 can be detected. For the inner PPM scheme, the I&D operation is tailored to the pulse duration $T_{\mathsf{p},2} = T_{\mathsf{p},1}/\bar{F}_{\mathsf{b}}$ with integration start $t_0 = t_k(\tilde{m}_2) - T_{\mathsf{p},2}/2$ and $t_k(\tilde{m}_2) := kT_{\mathsf{s}} + \tilde{m}_2 T_{\mathsf{p},2}$ ($\tilde{m}_2 \in \{0, 1, \ldots, 2\bar{F}_{\mathsf{b}} - 1\}$). In particular, is has to be known, in which pulse interval of the outer 2-PPM scheme the I&D receiver is supposed to search for a gap introduced by the inner PPM scheme and in which for a pulse. Note that the error probabilities for detecting a gap (with magnitude zero) within the outer 2-PPM pulse and for detecting a pulse (with magnitude $\sqrt{E_{\mathsf{s}}}$) within the unused pulse interval of the outer 2-PPM scheme are identical. For the purpose of our analysis we therefore assume that the received signal $r_{k,m_1,m_2}(t)$ is inverted for the time interval $\mathcal{T} = [kT_{\mathsf{s}} + \hat{m}_1 T_{\mathsf{p},1} - T_{\mathsf{p},1}/2, kT_{\mathsf{s}} + \hat{m}_1 T_{\mathsf{p},1} + T_{\mathsf{p},1}/2]$ prior to the I&D operation, i.e.,

$$\check{r}_{k,m_1,m_2}(t) := -\left(r_{k,m_1,m_2}(t) - \sqrt{E_{\mathsf{s}}}\right), \quad t \in \mathcal{T}. \tag{24}$$

By this means, the I&D operation is identical for all symbol hypotheses $\tilde{m}_2$. In the following, the additional SNR loss for the fast user due to the optical blue filter is not taken into account, in order to admit a direct comparison with the error performance of the slow receiver. If the outer PPM symbol m_1 is correctly detected (a-priori probability $1 - P_{\mathsf{s,e,nPPM-o}}$), the probability for correct detection of the inner $2\bar{F}_{\mathsf{b}}$-PPM symbol m_2 is associated with the event

$$\mathcal{E} = \bigwedge_{\tilde{m}_2 \neq m_2} \left\{\sqrt{E_{\mathsf{s}}/\bar{F}_{\mathsf{b}}} + w_{k,m_2} > w_{k,\tilde{m}_2}\right\}, \tag{25}$$

where $w_{k,m_2}, w_{k,\tilde{m}_2} \sim \mathcal{N}(0, N_0/2)$ are i.i.d. AWGN samples. Following the steps in the derivation of (23), the corresponding SEP of the inner PPM symbols is given by the expression $P_{\mathsf{e}}(1/\sqrt{\bar{F}_{\mathsf{b}}}, 2\bar{F}_{\mathsf{b}} - 1)$ for standard M-PPM with $M = 2\bar{F}_{\mathsf{b}}$. The SNR loss represented by $\gamma_{\mathsf{s}}/\bar{F}_{\mathsf{b}}$ is associated with the reduced integration time $T_{\mathsf{p},2} = T_{\mathsf{p},1}/\bar{F}_{\mathsf{b}}$ for the inner PPM scheme. If the outer PPM symbol m_1 is not correctly detected (a-priori probability $P_{\mathsf{s,e,nPPM-o}}$), the wrong time interval is inverted according to (24). In this case, the probability for correct detection of the inner $2\bar{F}_{\mathsf{b}}$-PPM symbol m_2 is associated with the event

$$\mathcal{E} = \bigwedge_{\tilde{m}_2 \neq m_2} \left\{-\sqrt{E_{\mathsf{s}}/\bar{F}_{\mathsf{b}}} + w_{k,m_2} > w_{k,\tilde{m}_2}\right\}, \tag{26}$$

leading to the SEP expression $P_{\mathsf{e}}(-1/\sqrt{\bar{F}_{\mathsf{b}}}, 2\bar{F}_{\mathsf{b}} - 1)$. We thus arrive at the final SEP expression (27) for the inner PPM scheme. The SEP (27) applies for the multicast case. In a broadcast scenario, however, the SEPs for the outer and inner PPM scheme need to be averaged. Correspondingly, the SEP of the fast receiver is obtained as

$$P_{\mathsf{s,e,nPPM-i,bc}} = (P_{\mathsf{s,e,nPPM-o}} + P_{\mathsf{s,e,nPPM-i}})/2 \tag{28}$$

in the broadcast case.

ACKNOWLEDGMENT

The authors would like to thank to Max Schurwanz and Juliane Kühnel (Hamburg University of Applied Sciences) for their initial investigations regarding a related hierarchical modulation scheme for VLC applications developed within the scope a thesis project. Furthermore, we acknowledge support for the article processing charge by the Open Access Publication Fund of Hamburg University of Applied Sciences (HAW).

REFERENCES

[1] S. Dimitrov and H. Haas, *Principles of LED Light Communications–Towards Networked Li-Fi*. Cambridge, U.K.: Cambridge Univ. Press, 2015.
[2] P. A. Hoeher, *Visible Light Communications–Theoretical and Practical Foundations*. Munich, Germany: Hanser Publishers, 2019.
[3] J. Mietzner et al., "Joint light planning and error-rate prediction for dual-use lighting/visible light communication," *IEEE Photon. J.*, vol. 14, no. 6, Dec. 2022, Art. no. 7362113.
[4] A. Tsiatmas, C. P. M. J. Baggen, F. M. J. Willems, J.-P. M. G. Linnartz, and J. W. M. Bergmans, "An illumination perspective on visible light communications," *IEEE Commun. Mag.*, vol. 52, no. 7, pp. 64–71, Jul. 2014.
[5] S. Rajagopal, R. D. Roberts, and S.-K. Lim, "IEEE 802.15.7 visible light communication: Modulation schemes and dimming support," *IEEE Commun. Mag.*, vol. 50, no. 3, pp. 72–82, Mar. 2012.
[6] *IEEE Standard for Local and Metropolitan Area Networks–Part 15.7: Short-Range Wireless Optical Communication Using Visible Light*, IEEE Standard 802.15.7-2018, Apr. 2019.
[7] *High-Speed Indoor Visible Light Communication Transceiver–System Architecture, Physical Layer and Data Link Layer Specification*," Recommendation ITU-T Standard G.9991, International Telecommunication Union, Geneva, Switzerland, 2019.
[8] J. Grubor, S. C. J. Lee, K.-D. Langer, T. Koonen, and J. W. Walewski, "Wireless high-speed data transmission with phosphorescent white-light LEDs," in *Proc. IEEE 33rd Eur. Conf. Exhib. Opt. Commun.*, 2007, pp. 1–2.
[9] J.-Y. Sung, C.-W. Chow, and C.-H. Yeh, "Is blue optical filter necessary in high speed phosphor-based white light LED visible light communications?," *Opt. Exp.*, vol. 22, no. 17, pp. 20646–20651, Aug. 2019.
[10] H. Jiang, P. A. Wilford, and S. A. Wilkus, "Providing local content in a hybrid single frequency network using hierarchical modulation," *IEEE Trans. Broadcast.*, vol. 56, no. 4, pp. 532–540, Dec. 2010.
[11] H. Sun, C. Dong, S. X. Ng, and L. Hanzo, "Five decades of hierarchical modulation and its benefits in relay-aided networking," *IEEE Access*, vol. 3, pp. 2891–2921, 2015.
[12] H. Li, Z. Huang, Y. Xiao, S. Zhan, and Y. Ji, "A power and spectrum efficient NOMA scheme for VLC network based on hierarchical pre-distorted LACO-OFDM," *IEEE Access*, vol. 7, pp. 48565–48571, 2019.
[13] C. Guerra-Yánez, A. Mederos-Barrera, S. Zvánovec, and Z. Ghassemlooy, "Experimental evaluation of a hierarchical QAM VLC system," in *Proc. IEEE 13th Int. Symp. Commun. Syst., Netw. Digit. Signal Proc.*, 2022, pp. 545–549.
[14] E. Guler, C. T. Geldard, I. Butler, T. Adiono, and W. O. Popoola, "3-D-hierarchical signalling for resilient optical wireless communication systems," *IEEE Open J. Commun. Soc.*, vol. 4, pp. 2870–2880, Oct. 2023.

[15] C. Zhu et al., "Hierarchical colour-shift-keying aided layered video streaming for the visible light downlink," *IEEE Access*, vol. 4, pp. 3127–3152, 2016.
[16] A. Tsiatmas, F. M. J. Willems, and C. P. M. J. Baggen, "Square root approximation to the Poisson channel," in *Proc. IEEE Int. Symp. Inf. Theory*, 2013, pp. 1695–1699.
[17] T. Komine and M. Nakagawa, "Fundamental analysis for visible-light communication system using LED lights," *IEEE Trans. Consum. Electron.*, vol. 50, no. 1, pp. 100–107, Feb. 2004.
[18] E. Schubert, *Light-Emitting Diodes*. 2nd ed., Cambridge, U.K.: Cambridge Univ. Press, 2006.
[19] J. Proakis and M. Salehi, *Digital Communications*, 5th ed. New York, NY, USA: McGraw-Hill, 2008.
[20] D. Tse and P. Viswanath, *Fundamentals of Wireless Communication*. Cambridge, U.K.: Cambridge Univ. Press, 2005.
[21] N. I. Miridakis and D. D. Vergados, "A survey on the successive interference cancellation performance for single-antenna and multiple-antenna OFDM systems," *IEEE Commun. Surveys Tuts.*, vol. 15, no. 1, pp. 312–335, First Quarter 2013.
[22] S. M. R. Islam, N. Avazov, O. A. Dobre, and K. Kwak, "Power-domain non-orthogonal multiple access (NOMA) in 5G systems: Potentials and challenges," *IEEE Commun. Surveys Tuts.*, vol. 19, no. 2, pp. 721–742, Second Quarter 2017.
[23] H. Schulze, J. Mietzner, and P. A. Hoeher, "Dispersive optical wireless indoor channels–from frequency-domain modeling to bit-error-rate prediction," *IEEE Photon. J.*, vol. 16, no. 1, Feb. 2024, Art. no. 7300713.
[24] S. Kasap, *Optoelectronics and Photonics—Principles and Practices.* 2nd ed., Pearson Education, 2013.
[25] Hamamatsu Photonics K. K., Si PIN photodiodes, S3590 series, 2024. [Online]. Available: https://www.hamamatsu.com/content/dam/hamamatsu-photonics/sites/documents/99_sales_library/ssd/s3590-08_etc_kpin1052e.pdf
[26] ReluxDesktop light planning software (relux informatik AG), 2022. [Online]. Available: https://reluxnet.relux.com/en/
[27] DIN EN 12464-1 (2021–11), "Light and lighting - Lighting of work places - Part 1: Indoor work places," 2021 (Table 3.76).
[28] *Spatial Distribution of Daylight - CIE Standard General Sky*, Joint ISO/CIE Standard ISO 15469:2004 (E)/CIE S. 011/E:2003, International Organization for Standardization, Geneva, Switzerland, 2003.